2D NMR Investigations of the Rotation of Axial Ligands in Six-Coordinate Low-Spin Iron(III) and Cobalt(III) Tetraphenylporphyrinates Having 2,6-Disubstituted Phenyl Rings: Quantitation of Rate Constants from ^{1}H EXSY Cross-Peak Intensities

Nikolai V. Shokhirev,*[1a,b] Tatjana Kh. Shokhireva,*[1a,c] Jayapal Reddy Polam,[1a] C. Todd Watson,[1a] Kamran Raffii,[2] Ursula Simonis,[2] and F. Ann Walker*[1a]

Department of Chemistry, University of Arizona, Tucson, Arizona 85721, and Department of Chemistry and Biochemistry, San Francisco State University, San Francisco, California 94132

Received: October 18, 1996; In Final Form: January 30, 1997[⊗]

Phase-sensitive NOESY/EXSY experiments have been utilized to measure the rates of axial ligand rotation for (tetramesitylporphyrinato)iron(III) and -cobalt(III) bis(2-methylimidazole), $[(TMP)Fe(2\text{-}MeImH)_2]^+ClO_4^-$ and $[(TMP)Co(2\text{-}MeImH)_2]^+BF_4^-$, and several related complexes at various low temperatures. The derivations of the expressions for EXSY cross-peak volumes (Ernst, R. R.; Bodenhausen, G.; Wokaun, A. *Principles of Magnetic Resonance in One and Two Dimensions*; Clarendon Press: Oxford, U.K., 1992; chapters 6 and 9) as a function of mixing time τ_m, longitudinal relaxation time T_1, and chemical exchange rate constant, k, have been extended to the case of cyclic four-site chemical exchange having a single rate constant. Cross-peak volumes were fit to the expressions, and the rate constants were calculated using a computer fitting program developed in this laboratory. The dependence of the reliability of the rate constant on T_1, τ_m, and other experimental factors is discussed. The temperature dependence of the rate constants was used to calculate the activation enthalpy and entropy for these complexes and two others, [tetrakis(2,6-dichlorophenyl)-porphyrinato]iron bis(2-methylimidazole) perchlorate, $[(2,6\text{-}Cl_2)_4(TPP)Fe(2\text{-}MeImH)_2]^+ClO_4^-$, and its 2,6-dibromophenyl analog, $[(2,6\text{-}Br_2)_4(TPP)Fe(2\text{-}MeImH)_2]^+ClO_4^-$, as well as the bis(1,2-dimethylimidazole) complexes of $(TMP)Co^{III}$. The values of $\Delta H^‡$ are very similar for all Fe(III) complexes (46−51 kJ/mol), and $\Delta S^‡$ values are close to zero. Nevertheless, the combined differences in these activation parameters led to rate constants for ligand rotation at 25 °C ranging from 1.1×10^5 (2,6-Br_2) to 1×10^4 (TMP) s^{-1}. For the $[(TMP)CoL_2]^+BF_4^-$ complexes where L = 2-MeImH and 1,2-Me_2Im, the values of $\Delta H^‡$ are very similar but slightly smaller than those for the low-spin Fe(III) complexes, but the values of $\Delta S^‡$ are rather negative (−63 and −84 J/(mol K), respectively), which lead to rate constants at 25 °C of 14 and 5 s^{-1}, respectively. The difference in $\Delta S^‡$ and thus the 10^3 difference in the rate constants for Fe(III) and Co(III) complexes probably indicates either steric hindrance to rotation of the 2-methyl group of the "hindered" ligand in the Co(III) complexes, where the Co−N_{ax} bond lengths are expected to be somewhat shorter than the corresponding Fe−N_{ax} bonds, or differences in solvation of the Co(III) complexes (BF_4^- anion) that lead to a more highly structured transition state than for those of the Fe(III) complexes (ClO_4^- anion). The methods developed for analysis of the EXSY data are general and could be used for any case of four-site chemical exchange with a single rate constant.

Introduction

The metal binding sites of heme proteins are extremely well-defined and include not only the porphyrinate nitrogens but also the axial ligand(s) provided to the metal by the protein. These protein-provided axial ligands have been shown to include the side chains of histidine, methionine, cysteine, tyrosine, and, in the case of cytochrome *f*, the N-terminal amino group of the polypeptide. Not only are these protein-provided side chains covalently attached to the protein backbone, but they are also held in precise orientations by protein structural constraints that include steric crowding of other protein side chains very near the heme, and, in the case of histidine ligands, hydrogen-bonding of the NH group of the imidazole ring to either amide carbonyl groups of the protein backbone or, possibly, hydrogen bond acceptors provided as amino acid side chains. Thus, in the heme proteins, there is essentially no possibility of rotation of the axial ligands about the metal−ligand bond. In contrast, it has long been assumed that, in model hemes in which axial ligands are not covalently attached to the porphyrinate ligand, axial ligand rotation is generally rapid at ambient temperatures. The question of how rapid ligand rotation is on "hindered" low-spin Fe(III) model hemes is the subject of this work.

Recently we have shown that ^{1}H NOESY/EXSY spectra of the bis(2-methylimidazole) (2-MeImH) complex of (tetramesitylporphyrinato)iron(III) chloride ($(TMP)Fe^{III}$) exhibit both NOE and chemical exchange cross-peaks.[3] We concluded that the multiple pyrrole-H, *ortho*-methyl, and *meta*-H mesityl resonances (four of each) arise from the binding of two bulky, unsymmetrical 2-methylimidazole ligands in perpendicular cavities above and below the metal, respectively,[3] as shown schematically in Figure 1. We also showed that the chemical exchange, or EXSY, cross-peaks result from rotation of the bulky axial ligands[3] at rates comparable to the 2D NMR time scale. Our proposed structure of this complex in solution, based upon the NOE cross-peaks observed at −74 °C where chemical exchange is suppressed,[3] has been corroborated recently by the report of the molecular structure of the corresponding bis(1,2-dimethylimidazole) complex of $(TMP)Fe^{III}$, determined by X-ray crystallography.[4] Since that time, Nakamura and co-workers[5] have published additional results that also corroborate our NOESY results and conclusions.

In our earlier NOESY investigation of the [(TMP)Fe(2-

[⊗] Abstract published in *Advance ACS Abstracts,* March 15, 1997.

S1089-5639(96)03234-3 CCC: $14.00

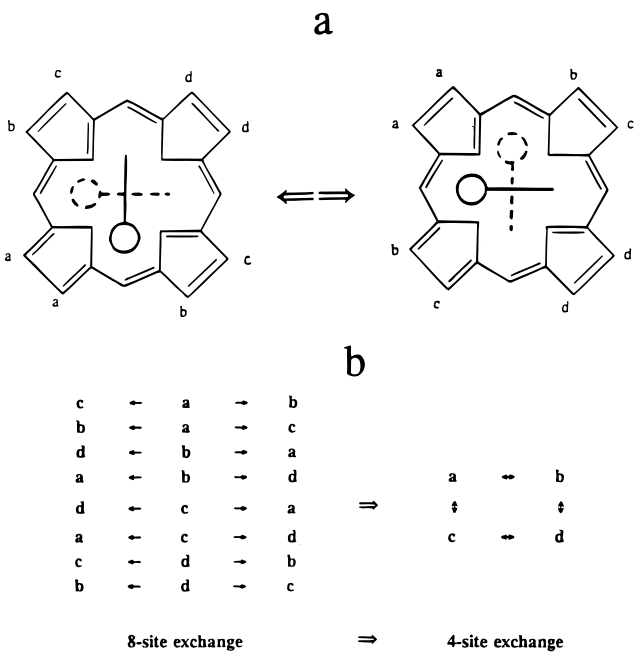

Figure 1. (a) Schematic representation of the four unique pyrrole-H created by the unsymmetrical 2-MeImH (or 1,2-Me_2Im) ligands and how they interchange upon one step of axial ligand rotation. (b) Catalog of the eight individual proton exchanges and their collapse to the four-site exchange case.

$MeImH)_2]^+Cl^-$ complex over the temperature range −29 to −74 °C,[3] we noted that the chemical exchange cross-peaks observed among both the set of four pyrrole-H and the set of four *ortho*-CH_3 resonances at intermediate temperatures (−54 °C) exhibited variations in intensity, for which several cross-peaks that had significant intensity at −29 °C were nearly unobservable at −54 °C.[3] More recent extensions of these investigations have made it clear that the cross-peak intensities contain information about both the rate of the chemical exchange process that produces the cross-peaks (axial ligand rotation) and confirmation of the assignment of the resonances of exchanging protons. In order to obtain this information we have extended the derivations of expressions for EXSY cross-peak intensities of Ernst and co-workers[6] to the case of cyclic four-site chemical exchange with a single rate constant. (This is a special case of four-site exchange for which full expressions can be derived in the manner of Ernst and co-workers,[6] unlike the more general and frequently-encountered cases in which there are unequal populations of the four sites and unequal rate constants for each transformation,[7−10] or more complex mechanisms for cases of equal populations, including those having two two-site exchanges of the same nuclei with different rate constants.[10,11]) We have used the derived expression to calculate the rate constants for rotation of the axial 2-MeImH ligands of [(TMP)-Fe(2-MeImH)$_2$]$^+$ClO$_4^-$ as a function of temperature and derived the activation enthalpy and entropy of rotation therefrom. We have found that the activation parameters obtained agree well with those reported previously for this system from line broadening analysis of the two *p*-CH_3 resonances at higher temperatures (−30 to +20 °C) using DNMR line shape fits.[12]

We have also extended these studies to the bis(2-methylimidazole) complexes of two other (perchlorato)iron(III) porphyrinates having bulky *ortho*-substituents, [*tetrakis*(2,6-dichlorophenyl)porphyrinato]iron(III), (2,6-Cl_2)$_4$(TPP)Fe^{III}, and [*tetrakis*(2,6-dibromophenyl)porphyrinato]iron(III), (2,6-Br_2)$_4$(TPP)-Fe^{III}, and to the (TMP)Co^{III} complexes of 2-MeImH and 1,2-Me_2Im, for which the NMR spectra indicate that ligand rotation is slow on the NMR time scale at room temperature. The results show that the rates of axial ligand rotation can be measured from EXSY cross-peak intensities for both paramagnetic d^5 iron(III) and diamagnetic d^6 cobalt(III) porphyrinates. Furthermore, the results allow interesting comparisons of rate constants and activation parameters to be made for the complexes of these two metals. The methods developed can be used for or extended to any other case of multisite chemical exchange with a single rate constant. In the accompanying study[13] we have used saturation transfer techniques to estimate the rate of ligand rotation for [(TMP)Fe(2-MeImH)$_2$]$^+$ClO$_4^-$ and have also calculated the barrier to rotation by molecular mechanics techniques. In another study,[14] we have extended our investigation of axial ligand rotation to diamagnetic cobalt(III) and iron(II) tetramesitylporphyrinates having other less hindered axial ligands and have investigated the extremely fast rotation of pyridine and unhindered imidazole ligands by dynamic NMR line shape analysis in the fast exchange regime.

Experimental Section

Materials and Methods. Syntheses of the iron(III)[15−17] and cobalt(III)[14,17,18] porphyrinates utilized for this study are described elsewhere. The 2-methylimidazole and 1,2-dimethylimidazole were purchased from Aldrich and used as received. Degassed samples of the bis-ligand iron(III) and cobalt(III) porphyrinate complexes (5−10 mM) with essentially no excess ligand present were prepared in 5 mm NMR tubes in deuterated methylene chloride, CD_2Cl_2 (Cambridge Isotope Laboratories), by dropwise addition of the axial base until the signals of the five-coordinate starting material had disappeared. Samples were then checked at low temperatures (<−40 °C) to be sure that very small signals from excess (uncoordinated) ligand were present.

^{1}H NMR spectra were recorded on a Varian Unity-300 spectrometer operating at 299.955 MHz. All spectra were recorded in CD_2Cl_2 over temperature ranges from −85 to +21 °C. The temperature was controlled by the Varian Unity-300 variable temperature accessory and was calibrated using the standard Wilmad methanol and ethylene glycol samples. The temperature remained stable to better than ±0.5 °C during the course of the NOESY (EXSY) experiments (2−4 h). The spectra were referenced to residual solvent protons (5.32 ppm relative to tetramethylsilane (TMS)). One-dimensional spectra were collected by using the standard one-pulse experiment with a spectral bandwidth of 10−12 kHz for Fe(III) complexes or 5 kHz for Co(III) complexes, a block size of 16K data points, a 30° pulse, and 32−64 transients. Phase-sensitive NOESY (EXSY) spectra were acquired over a bandwidth of 10−11 kHz (Fe(III)) or 4 kHz (Co(III)) using the ($90° - t_1 - 90° - \tau_m - 90° - t_2$) pulse sequence with 512 t_2 data points and 128 t_1 increments. Recycle delays ranged from 600 to 800 ms (Fe(III)) or from 2 to 2.3 s (Co(III)). The mixing times at each temperature were varied from 30 to 70 ms for Fe(III) and from 500 to 700 ms for Co(III). Usually, 32 transients were obtained for each t_1 increment. Data were processed with a Gaussian apodization function in both dimensions and zero-filled to give final matrices of 1024 t_1 × 1024 t_2 data points prior to Fourier transformation. Only NOESY/EXSY spectra that exhibited no cross-peaks between coordinated and residual free axial ligand were used, in order to eliminate contributions to the rate constants resulting from ligand exchange. Diagonal and cross-peak data were analyzed as described below.

Data Analysis

The processing of the EXSY experimental data is based on the modified Bloch equations.[6] The rotation of axial ligands

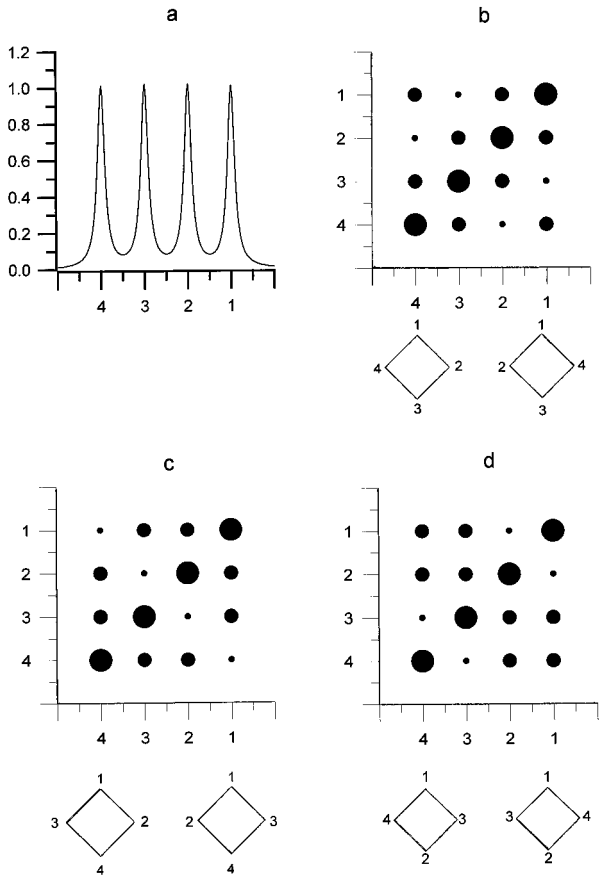

Figure 2. Computer simulation of the four-site chemical exchange process for four equally-separated exchanging peaks 1−4 observed in the 1D NMR spectrum, together with the three different possible 2D EXSY patterns that result from the possible spatial locations of the protons that give rise to the four resonances. Note that in each case there are four relatively weak cross-peaks and eight much stronger cross-peaks. These patterns result from "first-order" and "second-order" cross-peaks that depend upon the spatial relationship between the exchanging protons and thus which protons can exchange upon one (or more) step(s) of chemical exchange.

corresponds to the case of multiple-site exchange with equal rate constants. In particular, this is a four-site exchange with a rotation jump rate constant k. If the resonance lines are situated in increasing order and labeled with numbers 1−4, as shown in Figure 2, the three possible exchange schemes are

$$\begin{array}{ccc} 1 \leftrightarrow 2 & 1 \leftrightarrow 3 & 1 \leftrightarrow 3 \\ \updownarrow \quad \updownarrow & \updownarrow \quad \updownarrow & \updownarrow \quad \updownarrow \\ 4 \leftrightarrow 3 & 4 \leftrightarrow 2 & 2 \leftrightarrow 4 \end{array} \qquad (1)$$

and the corresponding kinetic matrices **K** are

$$\begin{pmatrix} -2k & k & 0 & k \\ k & -2k & k & 0 \\ 0 & k & -2k & k \\ k & 0 & k & -2k \end{pmatrix} \begin{pmatrix} -2k & 0 & k & k \\ 0 & -2k & k & k \\ k & k & -2k & 0 \\ k & k & 0 & -2k \end{pmatrix} \begin{pmatrix} -2k & k & k & 0 \\ k & -2k & 0 & k \\ k & 0 & -2k & k \\ 0 & k & k & -2k \end{pmatrix} \qquad (2)$$

Note that in a given molecule, different groups of nuclei (e.g., pyrrole-H, *ortho*-CH_3, and *meta*-H in metal porphyrinate complexes) may have different kinetic matrices (different "cases" in Figure 2) because the order of the proton resonances and the spatial relationship of the protons of each group may differ for one group of nuclei as compared to another, but yet have the same rate constant k. This is the situation for the systems described below.

The relaxation matrix **R** is diagonal with the following elements:

$$\mathbf{R}_{n,n} = 1/\mathrm{T}_{1n} \qquad (3)$$

where T_1 is the spin−lattice relaxation time for each site n. The kinetic and relaxation matrices form the dynamic matrix $\mathbf{L} = -\mathbf{R} + \mathbf{K}$.

The matrix of intensities **I** of the diagonal and all cross-peaks was calculated as an exponent of the dynamics matrix **L**:[6]

$$\mathbf{I} = \exp(\mathbf{L}\tau_\mathrm{m}) \qquad (4)$$

where τ_m is the mixing (exchange) time of the EXSY experiment. The above equation is valid up to some normalization (scaling) factor.

Hereafter the diagonal peaks are referred to as zero-order peaks. The off-diagonal peaks corresponding to terms k in the dynamic matrix are referred to as first-order peaks and, corresponding to zero terms, second-order peaks. This nomenclature originates from the series expansion of the matrix exponent

$$\mathbf{I} = 1 + \mathbf{L}\tau_\mathrm{m} + \frac{1}{2!}(\mathbf{L}\tau_\mathrm{m})^2 + \frac{1}{3!}(\mathbf{L}\tau_\mathrm{m})^3 + \ldots \qquad (5)$$

The first-order peaks appear if the first power of the matrix **L** is taken into account. The intensities of the second-order peaks are nonzero if at least the second power is taken into account (*or* beginning with the second power of the matrix **L**). The nth order terms in the expansion (5) represent the effect of n successive rotations (jumps). The schematic pictures of the 2D maps for all possible cases are presented in Figure 2. (As will be seen below, for all iron(III) porphyrinate complexes studied, the pyrrole-H resonances exhibit the pattern shown in Figure 2b; the *o*-CH_3 resonances of $[(\mathrm{TMP})\mathrm{Fe}(2\text{-MeImH})_2]^+\mathrm{ClO}_4^-$ exhibit the pattern shown in Figure 2c, while those of $[(\mathrm{TMP})\mathrm{CoL}_2]^+\mathrm{BF}_4^-$ (L = 2-MeImH and 1,2-Me_2Im) exhibit that shown in Figure 2d. Thus, the present study includes examples of all three patterns of weak and strong EXSY cross-peaks.)

Keeping the first three terms in eq 5 the intensities of the zero-, first-, and second-order peaks are obtained:

$$\mathbf{I}^0_{i,i} = \exp(-\tau_\mathrm{m}\langle 1/T_1\rangle)(1 - \tau_\mathrm{m}k(2 + \theta_i) + (\tau_\mathrm{m}k)^2(3 + 2\theta_i + \theta^2{}_i/2))$$

$$I^1_{i,j} = \exp(-\tau_\mathrm{m}\langle 1/T_1\rangle)(\tau_\mathrm{m}k + (\tau_\mathrm{m}k)^2[(\theta_i + \theta_j)/2 - 2])$$

$$\mathbf{I}^2_{i,j} = \exp(-\tau_\mathrm{m}\langle 1/T_1\rangle)(\tau_\mathrm{m}k)^2 \qquad (6)$$

where $\langle 1/T\rangle$ is the average of the inverse relaxation time over all four peaks, and

$$\theta_i = \frac{1}{k}\left(\frac{1}{T_{1i}} - \left\langle\frac{1}{T_1}\right\rangle\right) \qquad (7)$$

are the deviations of the reduced inverse relaxation times.

The above equations are valid for small exchange rates $k\tau_\mathrm{m} \ll 1$. For the general case, the matrix exponent should be calculated numerically, not necessarily by series expansion.

In the case of equal relaxation times T_1, the matrix exponent can be calculated analytically, and the intensities are

$$I^0_{i,i} = \frac{1}{4}\exp\left(-\frac{\tau_m}{T_1}\right)(1 + 2\exp(-2k\tau_m) + \exp(-4k\tau_m))$$

$$I^1_{i,j} = \frac{1}{4}\exp\left(-\frac{\tau_m}{T_1}\right)(1 - \exp(-4k\tau_m))$$

$$I^2_{i,j} = \frac{1}{4}\exp\left(-\frac{\tau_m}{T_1}\right)(1 - 2\exp(-2k\tau_m) + \exp(-4k\tau_m)) \quad (8)$$

Note that in this case, for any finite k and τ_m, $I^0 > I^1 > I^2$ and $I^0/I^1 = I^1/I^2$.

Fitting Procedure. The usual approach to the development of a fitting procedure, the least squares method, has been utilized in this work. For the case of 2D NMR spectra, it is necessary to minimize the sum of the squares of the deviations of experimental and theoretical intensities:

$$\sum_{n,m}^{\text{peaks}} |I^{\text{exper}}_{n,m} - cI^{\text{theor}}{}_{n,m}(k)|^2 W_{n,m} \Rightarrow \min \quad (9)$$

Here, c is a scaling factor, and $W_{n,m}$ are weights that reflect the accuracy of the measurements of intensities. Usually, such detailed information about the accuracy is not available. In particular, the peaks of different groups of nuclei have different magnitudes of intensities and different associated degrees of accuracy, and there is no obvious way to estimate the relative weights of the group contribution in the sum (9). Thus, the assumption of approximately equal accuracy was used, and weights in (9) were omitted. Also, different groups were fitted separately, and the results for each group were used for the additional estimation of the accuracy.

Experimentally integrated intensities are called "peak volumes", and from here on V is used instead of I^{exper}. For calculated quantities, the symbol I, omitting the superscript, is used. The linear parameter c can be easy obtained. Using matrix notation, c can be expressed as

$$c = \frac{\text{Tr}(\mathbf{V}\cdot\mathbf{I})}{\text{Tr}(\mathbf{I}^2)} \quad (10)$$

For this optimized value of c, the reduced mean square deviation is

$$\Delta(k) = 1 - \frac{\text{Tr}(\mathbf{V}\cdot\mathbf{I})^2}{\text{Tr}(\mathbf{I}^2)\text{Tr}(\mathbf{V}\cdot\mathbf{V}^{\text{T}})} \quad (11)$$

and must be minimized with respect to k (in general, numerically).

For the different compounds studied and the different temperatures employed, the experimental rate constants may differ by several orders of magnitude. For the trial value of the rate constant k, the assumption of equal relaxation times was used. (However, in the later analysis the actual individual relaxation times were used.) Using expressions 8 with $I = V$, the minimization of $\Delta(k)$ can be done analytically:

$$k = \frac{1}{2\tau_m}\ln(f + [f^2 + 1]^{1/2}) \quad (12)$$

$$f = \frac{S_1}{S_0 - S_2}$$

Here S_n are the sums of the nth order peak intensities. In particular, for Case 1,

$$S_0 = V_{11} + V_{22} + V_{33} + V_{44}$$

$$S_1 = V_{12} + V_{21} + V_{23} + V_{32} + V_{34} + V_{43} + V_{14} + V_{41}$$

$$S_2 = V_{13} + V_{31} + V_{24} + V_{42}$$

For perfect experiments ($V = I$) with different relaxation times for each peak, estimation 12 differs from the actual value by the second-order deviations in inverse relaxation times, at least for the case of small $k\tau_m$. Using expressions 6 and 7, it can be shown that estimation 12 should be corrected by multiplying by the factor $1 + \kappa$, where

$$\kappa = (\theta_1{}^2 + \theta_2{}^2 + \theta_3{}^2 + \theta_4{}^2)/8 \quad (13)$$

For ideal experiments, including correct calculation of peak intensities, the value of the deviation Δ (eq 11) at optimal rate constant k_0 must be equal to zero: $\Delta(k_0) = 0$. Thus, in real experiments, the value of $\Delta(k_0)$ can be considered as a measure of relative accuracy. As another measure of accuracy, the "flexibility" δk was calculated. It is defined as follows:

$$\frac{\Delta(k_0 \pm \delta k)}{\Delta(k_0)} - 1 = \zeta \quad (14)$$

For the level of flexibility ζ, the value 0.25 was chosen. In other words, all values of k in the interval $k_0 \pm \delta k$ are considered as equally reproducing experimental intensities within the deviation of discrepancy $\zeta\ \Delta(k_0)$.

It is also necessary to check to which case the matrix $V_{n,m}$ of input experimental volumes matches better. According to eqs 6−8, for accurate data the following set of inequalities should be observed:

$$S_0 > S_1/2 > S_2 \quad (15)$$

If the assignment to the cases 1−3 is incorrect for an individual experiment (one with a particular mixing time and temperaure), then

$$S_0 > S_2 > S_1/2 \quad (16)$$

instead of (15). If this check gives an assignment different from the well-established case (that deduced for other temperatures or mixing times), then these data should be considered noisy and unreliable.

Calculation of 2D Intensities. For accurate comparison of experimental peak volumes, the 2D intensities in the x,y-plane of the EXSY maps were calculated according to the expression

$$I(x,y) = \sum_{n,m=1} I_{n,m}\tilde{T}_{2n}\tilde{T}_{2m}[1 + (x - \delta_n)^2\tilde{T}_{2n}{}^2]^{-1}[1 + (y - \delta_m)^2\tilde{T}_{2m}{}^2]^{-1} \quad (17)$$

Here $I_{n,m}$ are the elements of the matrix (4), and the reduced transverse relaxation time is introduced

$$\tilde{T}_2 = 10^{-6}T_2\omega_0 \quad (18)$$

where ω_0 is the frequency of the NMR spectrometer in angular frequency units. The theoretical volumes of the peaks were calculated by integration over appropriate rectangular areas.

TABLE 1: Numerical Experiments Involving Different Methods of Integration. (Model Parameters: $\tau_m = 40.0$ ms; T_2, $T_1 = 50.0$ ms; "Noise" Level $\epsilon = 0.001$(Max Amplitude); Distance between Peaks, Set at 3 ppm)

rate constant, k (s^{-1})	integrated intensities I^0	I^1	I^2	$k\tau_m$
100.0	0.112 408[a]	0.112 332[a]	0.112 257[a]	4.0
10.0	0.236	0.0897	0.0341	0.4
1.0	0.415	0.0166	0.000664	0.04
0.1	0.446	0.00178	0.000007	0.004

input rate constant	output rate constant (calculated error[b]) case 1	case 2	case 3
First Method of Integration (Rectangular Area to Nearest Saddle Points)			
100.0	100.03 (0.034%)[a]	100.02 (0.024%)[a]	100.06 (0.006%)[a]
10.0	10.02 (0.216%)	10.03 (0.27%)	10.03 (0.027%)
1.0	1.016 (1.65%)	1.016 (1.57%)	1.013 (1.29%)
0.1	0.111 (10.8%)	0.110 (9.78%)	0.108 (7.61%)
Second Method of Integration (Within Boundaries at the "Noise Level" Near a Saddle Point)			
100.0	100.01 (0.013%)[a]	100.02 (0.016%)[a]	100.02 (0.018%)[a]
10.0	9.70 (−2.95%)	9.70 (−2.95%)	9.71 (−2.95%)
1.0	0.842 (−15.8%)	0.842 (−15.8%)	0.841 (−15.9%)
0.1	0.0464 (−46.4%)	0.0462 (−53.9%)	0.0459 (−54.1%)

[a] Calculations done without rounding off what would be insignificant figures in experimental work. [b] Deviation between input and output values.

In the numerical experiments and in the processing of experimental data the following variants of the calculations of I_{nm}, used in eq 11, were employed: (i) net integral intensities (4) (perfect integration); (ii) integration over a rectangular area with the center at a peak and boundaries at the nearest saddle point of the intensity map (first method); (iii) integration within boundaries at a "noise" level that is near the saddle point (second method) (in most cases, this will be a smaller integration area than that for the first method, which will thus result in cutting off the wings of the (broad) peaks).

Numerical Experiments. For comparison of the two methods of calculation of peak volumes, the following numerical experiments were performed: For several relaxation and mixing times (for simplicity T_1s were assumed to be equal) and different values of $k\tau_m$, the integrated intensities were calculated according to eq 8. These intensities were used for the calculation of two-dimensional amplitudes (eq 14). Then the integrated peak volumes were inserted into eqs 12. We will refer to rate constants calculated in such a way as "output" rates. A typical example of such numerical experiments is presented in Table 1, and the main results can be summarized as follows.

For $k\tau_m > 0.1$ and typical experimental values of relaxation times and distances between peaks, the first method of integration reproduces the input rate constants with errors of about 1%. For more closely spaced peaks the error may be large.

The accuracy of the second method depends on the chosen noise level ϵ. For well resolved peaks, the errors in determination of the volumes of nth order peaks are estimated according to the relationship $\delta V^n = (4/\pi)[\epsilon I^0/I^n]^{1/2}$. The level $\epsilon = 0.001$ gives an error of 4% of the zero-order peak volumes. Note that for more rapidly decaying line shapes than those in (14), the same accuracy of integration corresponds to a higher noise level. For example, for a Gaussian line $\epsilon = 0.06$ should be chosen instead of 0.001 for a Lorentzian line. The second method for $k\tau_m > 0.1$ and the chosen accuracy of integration reproduces rate constants with errors less than 10%.

In ideal experiments (exact determination of intensities) there are no upper limits for the value $k\tau_m$. But the upper boundary

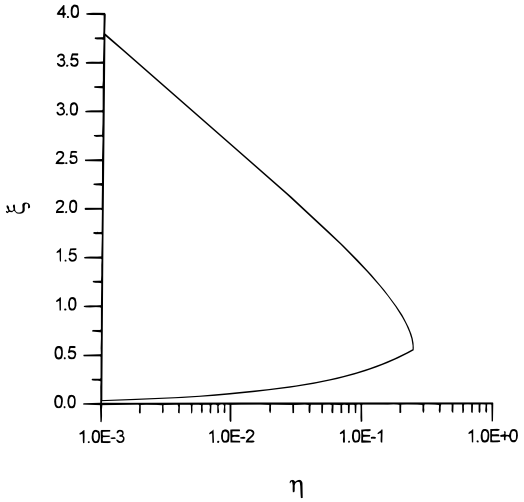

Figure 3. Dependence of the lower and upper limits for the optimal $\xi = k\tau_m$ upon the accuracy $\eta = 2\epsilon/I^0$, where 1.0E−3, for example, represents 1.0×10^{-3}.

TABLE 2: Boundaries for ξ (Equation 21)

η	ξ_{min}	ξ_{max}	η	ξ_{min}	ξ_{max}
0.01	0.10	2.64	0.05	0.23	1.80
0.02	0.14	2.29	0.10	0.33	1.41
0.03	0.17	2.08	0.25	0.5493	

of $\xi = k\tau_m$ depends on the accuracy of the measurements. The optimum condition for the extraction of the rate constant should be

$$V^0 \gg V^1 \gg V^2 \gg \epsilon \tag{19}$$

where ϵ is the experimental error. The sign $\gg$ indicates that intensities differ more than experimental errors. The simple conditions

$$\begin{aligned} I^0 - \epsilon &> I^1 + \epsilon \\ I^1 - \epsilon &> I^2 + \epsilon \\ I^2 - \epsilon &> \epsilon \end{aligned} \tag{20}$$

instead of inequalities 17 together with expressions 8 for the intensities give the following limits for ξ:

$$\ln\left(\frac{1+\eta^{1/2}}{1-\eta^{1/2}}\right) < 2\xi < \ln\left(\frac{2+\eta}{1-\eta-[1-4]^{1/2}}\right) \tag{21}$$

where the reduced error $\eta = 2\epsilon/I^0$. The boundaries for ξ are plotted in Figure 3 and tabulated in Table 2 for selected values of η. Conditions 21 for the mixing time implicitly depend on relaxation times *via* I^0. Roughly, the optimal mixing time is of the order of the inverse rate constant, and the larger the error, the more rigid these conditions are. The maximum value of η is $^1/_4$, and at this point $\xi_{min} = \xi_{max} = 0.5493$. Note that if the other confidence interval $n\epsilon$ is chosen in (20) instead of 2ϵ ($\pm\epsilon$), then 2ϵ should be substituted by $n\epsilon$ in the definition of η.

For the first method of integration, the output rates are overestimated. This reflects the overlap of peaks, and the weaker the cross-peaks, the more contribution from larger peaks (mainly from zero-order peaks), and, consequently, the more the overestimation of the rate constant. In other words, this method underestimates the input rate constant for the case of perfect integration of the volumes.

The second method of integration underestimates the output rate constants because of underestimation of cross-peaks.

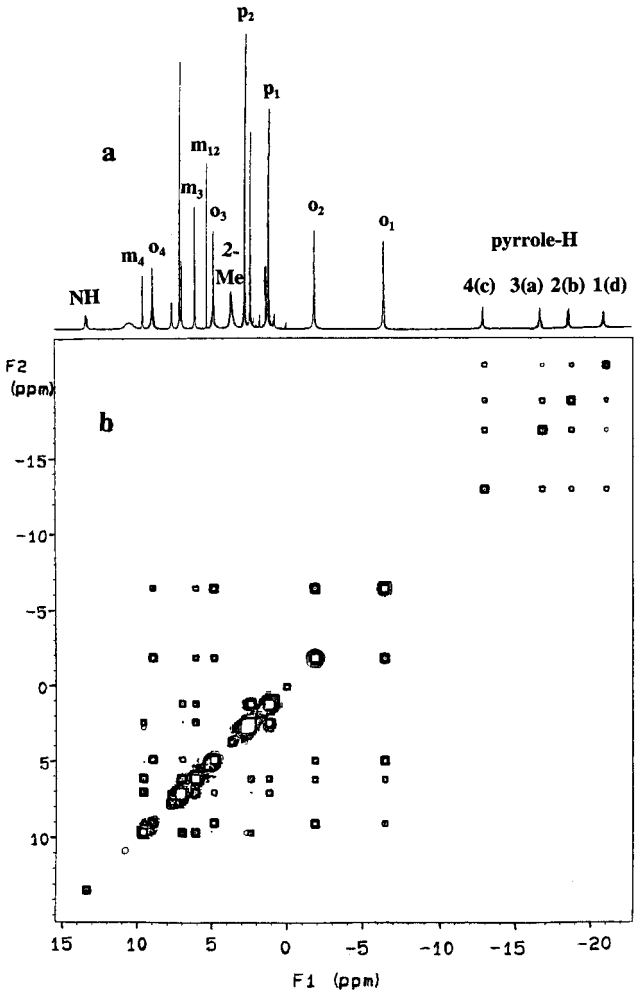

Figure 4. (a) 1D ^{1}H NMR spectrum of $[(TMP)Fe(2\text{-}MeImH)_2]^+ClO_4^-$ at −55 °C. (b) Magnitude NOESY/EXSY spectrum at the same temperature. Experimental conditions: spectral bandwidth, 11467.9 Hz; number of transients, 32; data points in t_2, 512; number of t_1 increments, 128; mixing time (τ_m), 70 ms; final 2D matrix size, 1024 × 1024. In this case, the spectrum was symmetrized, though for the measurement of rate constants the spectra were not symmetrized. Note the 4 × 4 matrix of chemical exchange cross-peaks for pyrrole-H, *ortho*-CH_3, and *meta*-H resonances.

Consequently, this method overestimates the input rate constant for the case of perfect integration of the volumes.

Fitting Program. The above described procedures were accomplished by creating a program for an IBM-type PC. The input parameters can be introduced either in a program menu or in an input file. The calculated values are displayed on the screen and may be written to an output file. In addition, the program provides a visual control of fitting by plotting an intensity contour map.

NMR Experimental Results

The computer simulation of the four-site chemical exchange process shown in Figure 2 for four equally-separated exchanging peaks 1−4 observed in the 1D NMR spectrum demonstrates the three different possible 2D EXSY patterns that result from the possible exchange relationships of the protons that give rise to the four resonances. In each case, four of the twelve EXSY cross-peaks are predicted to be weaker than the other eight, since protons opposite each other can only exchange after more than one step of ligand rotation or other cyclic chemical exchange process. In Figure 4 are shown the 1D and magnitude NOESY/EXSY spectra of $[(TMP)Fe(2\text{-}MeImH)_2]^+ClO_4^-$ in CD_2Cl_2 at −55 °C, recorded with a mixing time of 70 ms (chosen to show the differences in chemical exchange cross-peak intensities within each group). The 4 × 4 patterns of chemical exchange cross-peaks for the pyrrole-H (−13 to −21 ppm) and mesityl *o*-CH_3 (+9 to −7 ppm) are clearly evident in this spectrum, whereas the 4 × 4 pattern of mesityl *m*-H resonances (+9.5 to + 6 ppm), for which two resonances overlap at 6 ppm, is less evident, though present. For the pattern of *o*-CH_3 cross-peaks it can be seen that those between resonances 1 and 4 and between 2 and 3 are weaker than the other eight cross-peaks. This identifies the methyl resonances as belonging to the pattern shown in Figure 2c. In comparison, within the pattern of pyrrole-H cross-peaks it can be seen that the 1,3 and 3,1 cross-peaks are weaker than the others, suggesting that the exchange pattern shown in Figure 2b is observed. However, cross-peaks 2,4 and 4,2 are not as weak as the 1,3 and 3,1 cross-peaks, as would be expected by the pattern shown in Figure 2b. This is because the pyrrole protons that give rise to resonances 2 and 4 also exhibit NOE cross-peaks due to their spatial proximity, as reported previously.[3] At higher temperatures and shorter mixing times, the NOE contribution is significantly diminished relative to the chemical exchange contribution, and all four cross-peaks, 1,3; 2,4; 3,1; and 4,2, can be used for calculation of rate constants. Both of the EXSY patterns observed are in complete accord with our earlier assignment of the spectrum of this complex,[3] which was based upon the pattern of NOE cross-peaks observed at −74 °C, where chemical exchange is suppressed: On the basis of the observed NOE cross-peaks, pyrrole-H resonances 2 and 4 were assigned to inequivalent protons within a single pyrrole ring (protons b and c of Figure 1), of which there are two equivalent rings opposite each other; these protons cannot interchange magnetic environments upon one step of ligand rotation. Likewise, resonances 1 and 3 were assigned to pairs of equivalent protons in each of two opposite pyrrole rings, and again, these protons cannot interchange magnetic environments upon one step of ligand rotation. For the *o*-CH_3 resonances, we had assigned *o*-1 and *o*-3 to the same mesityl ring on the basis of the NOE conectivity to *meta*-H and *para*-CH_3 resonances, and likewise, *o*-2 and *o*-4 to another mesityl group.[3] In each case, *ortho*-methyls within a given mesityl ring cannot exchange magnetic environments upon one step of ligand rotation, but methyls on adjacent rings can. Thus, the *o*-1 of one mesityl ring can exchange with the *o*-3 of the adjacent ring, and the same for *o*-2 and *o*-4. The signals that *cannot* exchange upon one step of rotation are *o*-1 (top) and *o*-4 (bottom), and likewise *o*-2 (top) and *o*-3 (bottom). In each case, these are methyl groups on adjacent rings that cannot interchange. However, two-step rotation brings *o*-1 (top) to *o*-4 (top) and *o*-2 (top) to *o*-3 (top), thus achieving the chemical exchange in two steps. The intensities of the chemical exchange cross-peaks in Figure 4 thus completely support the earlier assignments.[3]

To measure the rates of ligand rotation from EXSY cross-peak volumes, we have utilized phase-sensitive NOESY/EXSY experiments. The complexes of this study are of a size that puts them very close to the T_1 minimum at a 300 MHz proton frequency. Interestingly, we found the NOE cross-peaks to have the same phase as the diagonal for all iron(III) perchlorate complexes (negative NOEs), for which spectra were recorded at low temperatures, but the opposite phase to the diagonal peaks for both cobalt(III) tetrafluoroborate complexes (positive NOEs), for which spectra were recorded above 0 °C. In both cases, chemical exchange cross-peaks have the same phase as the diagonal peaks. In principle, ROESY cross-peak intensities could also have been used for measurement of chemical

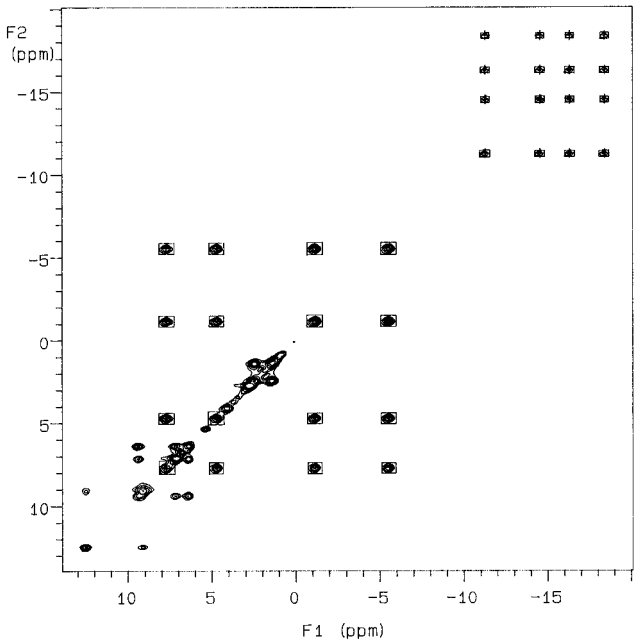

Figure 5. Measurement of diagonal and cross-peak intensities of EXSY spectra of $[(TMP)Fe(2\text{-}MeImH)_2]^+ClO_4^-$ at −36 °C from a phase-sensitive experiment for (a) the pyrrole-H and (b) the *o*-CH_3 resonances, allowing calculation of a rate constant in each case. From this data set, $k = 29\ s^{-1}$ for a and $23\ s^{-1}$ for b.

exchange rate constants, but for the paramagnetic complexes with chemical shift ranges of up to 40 ppm, we have found that ROESY spectra are difficult to phase across the entire spectrum, and thus it is difficult to measure cross-peak volumes reliably. Such spectral phasing problems were not encountered in the phase-sensitive NOESY/EXSY experiments.

In Figure 5 is shown an example of a phase-sensitive NOESY/EXSY spectrum for $[(TMP)Fe(2\text{-}MeImH)_2]^+ClO_4^-$ at −36 °C, recorded with a mixing time of 30 ms. At this temperature, the NOESY/EXSY cross-peak intensities are dominated by chemical exchange, so that contributions from the NOE between pyrrole-H resonances 2 and 4 are negligible. Diagonal and cross-peak volumes were obtained using the Unity-300 software and were used in eq 5 to calculate the rate constant, *k*, from the pyrrole-H set and also from the *o*-CH_3 set of chemical exchange cross-peaks. For the example shown in Figure 5, $k = 29$ and $23\ s^{-1}$, respectively. For each temperature, several EXSY maps were obtained, each with a different mixing time. In some cases it was found that better EXSY maps could be obtained if the mixing times were optimized for either one or the other type of protons, since the pyrrole-H resonances have much shorter relaxation times T_1 and T_2 than do the *o*-CH_3 resonances. All values of *k* and the resultant average *k* values for each type of proton at each temperature were used to construct an Eyring plot. In general, the pyrrole-H matrix of cross-peaks gave slightly larger rate constants than did the *o*-CH_3 matrix.

Similar EXSY studies were also carried out on $[(2,6\text{-}Cl_2)_4(TPP)Fe(2\text{-}MeImH)_2]^+ClO_4^-$ and $[(2,6\text{-}Br_2)_4(TPP)Fe(2\text{-}MeImH)_2]^+ClO_4^-$, also in in CD_2Cl_2. In these cases, only the pyrrole-H resonances were available for calculation of the rate constants. The pyrrole-H chemical shifts and cross-peak intensity patterns are very similar to those shown in Figures 4 and 5, and the rate constants measured from the phase-sensitive NOESY/EXSY maps at the temperatures and mixing times chosen are similar in magnitude to those for $[(TMP)Fe(2\text{-}MeImH)_2]^+ClO_4^-$, though in general the rate constants at a given temperature are approximately a factor of 10 larger than those for the corresponding TMP complex. (Comparative Eyring plots

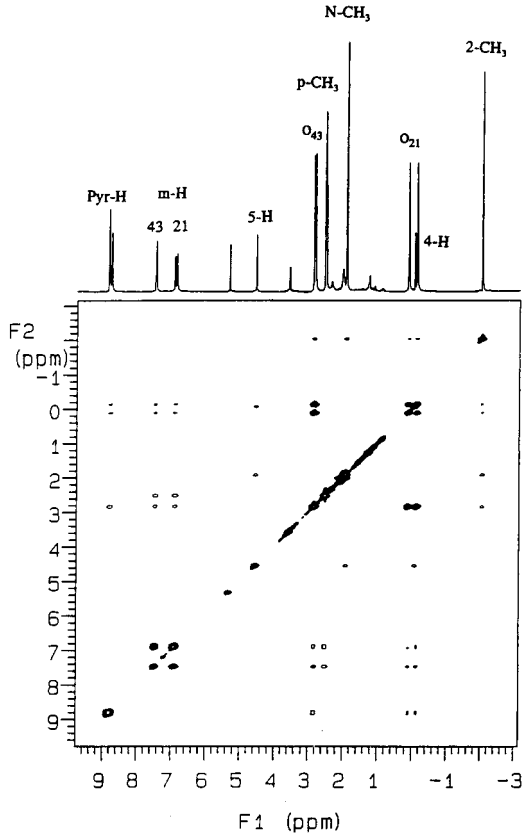

Figure 6. Phase-sensitive NOESY/EXSY spectrum of $[(TMP)Co(1,2\text{-}Me_2Im)_2]^+BF_4^-$ at 10 °C, showing EXSY cross-peaks with the same phase (multiple contour circles) as the diagonal and NOE cross-peaks with the opposite phase (single contour circles). At lower temperatures the cross-peaks between the two *o*-CH_3 resonances near 0 ppm weaken with respect to the cross-peaks between each of them and the two very closely spaced *o*-CH_3 cross-peaks near 3 ppm, indicating that the cross-peak pattern shown in Figure 3d (case 3) is observed in this case. The same pattern is observed for the related $[(TMP)Co(2\text{-}MeImH)_2]^+$ complex.

are shown in Figure 7 below; rate constants and activation parameters are provided in Table 4 below, and are discussed in Discussion.)

In Figure 6 is shown an example of a phase-sensitive NOESY/EXSY spectrum for $[(TMP)Co(1,2\text{-}Me_2Im_2)]^+BF_4^-$ at 10 °C, recorded with a mixing time of 700 ms. The pyrrole-H resonances, all very close together near 8.8 ppm, could not be used to measure the rate constant for ligand rotation. Although two of the *o*-CH_3 resonances are nearly overlapping at 2.8 ppm, it was still possible to estimate the chemical exchange rate constant from the observed cross-peak intensities. From the *o*-CH_3 cross-peak intensities of the example spectrum shown in Figure 6, $k = 1.5\ s^{-1}$.

Fitting Results. *Primary Fitting.* For the determination of rate constants the above described procedure was used. Unreliable points were dropped ((*i*) wrong case; (*ii*) deviation of more than 30% from the initial guess; (*iii*) large flexibility).

Secondary Fitting. The rate constants obtained were used for the determination of $\Delta H^{\ddagger}$ and $\Delta S^{\ddagger}$. The dependencies of $\ln(kh/k_BT)$ on inverse temperature were plotted, and ordinary linear regression (least squares)[19] fitting was applied. The slope and intercept of the linear fit were assigned to $\Delta H^{\ddagger}$ and $\Delta S^{\ddagger}$, respectively, according to the equation

$$\ln\left(\frac{kh}{k_BT}\right) = -\frac{\Delta H^{\ddagger}}{RT} + \frac{\Delta S^{\ddagger}}{R} \qquad (22)$$

TABLE 3: Eyring Activation Enthalpies, Entropies, Free Energies, and Rate Constants at 298 K for $[(TMP)Fe(2\text{-}MeImH)_2]^+$ Obtained from Fitting Methods 1−4

fitting method[a]	$\Delta H^{\ddagger}$ (kJ/mol)	$\Delta S^{\ddagger}$ (J/(K mol))	$\Delta G^{\ddagger}_{298}$ (kJ/mol)	k_{298} s^{-1}
1	51.5	3.0	50.6	8.6×10^3
2	51.0	2.0	50.6	9.1×10^3
3	51.0	2.6	50.2	9.7×10^3
std dev	3.3	14.6	7.5	
4	48.1	−9.6	51.0	7.3×10^3
5	61.8	51.9	46.3	4.8×10^4
6	54.0	15.5	49.4	1.4×10^4

"flexibility" 16−43%
max T_1 correction 14%
range of $\ln(kh/k_BT)$ 2.8

[a] Methods 1, simple estimation (eq 12); 2, fitting of intensities (eq 4); 3, first integration method (integration to the nearest saddle point; this method is felt to give the most reliable rate constants (see text); 4, second integration method (integration to the "noise" level 0.1%); 5, saturation transfer measurements;[13] 6, reference 12.

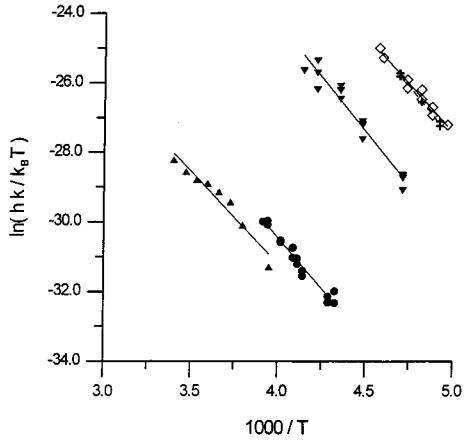

Figure 7. Eyring plots for all systems studied: ▼, $[(TMP)Fe(2\text{-}MeImH)_2]^+ClO_4^-$; ◊, $[(2,6\text{-}Cl_2)_4(TPP)Fe(2\text{-}MeImH)_2]^+ClO_4^-$; +, $[(2,6\text{-}Br_2)_4(TPP)Fe(2\text{-}MeImH)_2]^+ClO_4^-$; ●, $[(TMP)Co(2\text{-}MeImH)_2]^+BF_4^-$; and ▲, $[(TMP)Co(1,2\text{-}Me_2Im)_2]^+BF_4^-$.

The ranges of the variations of $\ln(kh/k_BT)$ are 1.9−3.1 for the systems studied (see Tables 3 and 4). Standard deviations for $\Delta H^{\ddagger}$ and $\Delta S^{\ddagger}$ were calculated.[19] All data and linear fitting, corresponding to the first integration method, are summarized in Figure 7 and Table 4.

Discussion

The Eyring plots for all systems studied are shown in Figure 7. From the Eyring plot for $[(TMP)Fe(2\text{-}MeImH)_2]^+ClO_4^-$ a value of $\Delta H^{\ddagger} = 51.0 \pm 3.3$ kJ/mol and $\Delta S^{\ddagger} = 3 \pm 15$ J mol^{-1} K^{-1} were obtained from the first integration method (fitting method 3 of Table 3), which is the one that is considered to be most reliable. In comparison, the simple estimation method (eq 12, fitting method 1 of Table 3) gives excellent agreement, as does fitting of intensities (eq 4, fitting method 2). The values obtained from the second integration method (method 4, Table 3), however, differ somewhat from those obtained using methods 1−3. As mentioned above, the second integration method underestimates the calculated rate constants because of underestimation of cross-peak intensities. The results obtained from methods 1−3, Table 3, compare favorably with those obtained from saturation transfer measurements on the same complex presented in the accompanying paper[13] and with those obtained previously from line broadening measurements of the two mesityl *p*-CH_3 signals using the DNMR line shape fitting program, $\Delta H^{\ddagger} = 54.0 \pm 1.7$ kJ/mol and $\Delta S^{\ddagger} = 15.5 \pm 6.7$ J mol^{-1} K^{-1},[12] even though the extrapolated rate constant k_{298} is somewhat larger. However, this is not surprising because the temperature for tabulation of the rate constants is fairly far out of the range of temperatures used for the measurements by either DNMR, saturation transfer, or EXSY cross-peak intensities, and thus extrapolation magnifies small differences in the Eyring activation quantities. We have chosen 298 K as the reference temperature for comparing the rate constants mainly to emphasize the rapid rate of ligand rotation at room temperature, a finding in contradiction to earlier results that suggested that less-hindered pyridine ligands bound to (TPP)Co(III) do not rotate at room temperature.[20]

Numerical rate and activation data for all complexes studied are summarized in Table 4. For the two $[(2,6\text{-}X_2)_4(TPP)Fe(2\text{-}MeImH)_2]^+ClO_4^-$ complexes (X = Cl, Br), the average values of $\Delta H^{\ddagger}$ are slightly smaller than that for the TMP complex, although the values for all three iron(III) porphyrinate complexes with 2-methylimidazole are within experimental error of each other. This suggests that all three complexes are similarly ruffled, such that the *ortho*-substituents do not actually contact the rotating 2-methylimidazole ligand in each case, and hence the $\Delta H^{\ddagger}$ is not influenced by the actual size of the *ortho*-substituent; as we have shown elsewhere,[21] the energy barrier to ruffling of the porphyrin ring is extremely small. In all cases the calculated values of $\Delta S^{\ddagger}$ are smaller than the experimental error in measuring the activation entropy, and thus we can conclude that $\Delta S^{\ddagger}$ is nearly zero for these low-spin Fe(III) complexes.

In contrast, for the $[(TMP)CoL_2]^+BF_4^-$ complexes, while the activation enthalpies are not very different from those of the Fe(III) complexes, the values of $\Delta S^{\ddagger}$ are negative and fairly large in magnitude (−62 (2-MeImH) and −84 (1,2-Me_2Im) J/(mol K), respectively). The relatively large, negative values of $\Delta S^{\ddagger}$ for the Co(III) complexes may either be a result of the slightly (∼0.05 Å) shorter $M-L_{ax}$ bond lengths for this metal,[22] which may lead to hindered rotation of the 2-methyl group of the imidazole ligands during the process of axial ligand rotation, or they may result from differences in solvation of the Co(III) complexes in the transition state from those of the Fe(III) complexes. It should be noted that all of the Fe(III) complexes utilized perchlorate as counterion, while the Co(III) complexes utilized tetrafluoroborate. Although both of these ions are tetrahedral and of similar size, the BF_4^- ion is slightly smaller, which may lead to stronger solvation, a larger rotating unit in solution, and the necessity of more structural reorganization in the transition state; in support of this explanation, the value of $\Delta S^{\ddagger}$ for rotation of 4-(dimethylamino)pyridine ligands in $[(TMP)Co(4\text{-}NMe_2Py)_2]^+BF_4^-$ (measured by DNMR methods

TABLE 4: Comparison of Activation Enthalpies, Entropies, Room Temperature Free Energies, and Rate Constants Obtained from Fitting Method 3 for All Complexes Studied

complex	$\Delta H^{\ddagger}$ (kJ/mol)	$\Delta S^{\ddagger}$ (J/(K mol))	$\Delta G^{\ddagger}_{298}$ (kJ/mol)	k_{298} s^{-1}	range of $\ln(kh/k_BT)$ studied
$[(TMP)Fe(2\text{-}MeImH)_2]^+ClO_4^-$	51.0 ± 3.3	3 ± 15	50 ± 8	1×10^4	2.8
$[(2,6\text{-}Cl_2)_4(TPP)Fe(2\text{-}MeImH)_2]^+ClO_4^-$	46.4 ± 3.8	4 ± 18	45 ± 9	7×10^4	2.2
$[(2,6\text{-}Br_2)_4(TPP)Fe(2\text{-}MeImH)_2]^+ClO_4^-$	49.0 ± 1.8	15 ± 8	44 ± 3	10×10^4	1.9
$[(TMP)Co(2\text{-}MeImH)_2]^+BF_4^-$	48.1 ± 2.6	−62 ± 11	67 ± 5	14	2.3
$[(TMP)Co(1,2\text{-}Me_2Im)_2]^+BF_4^-$	43.9 ± 4.6	−84 ± 16	69 ± 10	5	3.1

in the fast exchange regime[14]) is of very similar magnitude (−60 J mol^{-1} K^{-1}).

As a result of the difference in $\Delta S^{\ddagger}$, the rates of ligand rotation for the Fe(III) complexes are between 3 and 4 orders of magnitude faster (k_{298} ∼10^4−10^5 s^{-1}) than those of the corresponding Co(III) complexes (k_{298} ∼5−14 s^{-1}). The fast rate of ligand rotation for the low-spin d^5 Fe(III) complexes has prevented us from using 2-MeImH complexes of tetrakis-(2,6-disubstituted phenyl)porphyrinates to estimate the reduction potentials of iron(III) porphyrinates having perpendicular axial ligands, a long-range goal of this research. Furthermore, in a study of the rate of rotation of pyridine and *nonhindered* imidazole ligands about the ligand−cobalt bonds of [(TMP)-CoL_2]$^+$ we have found that, contrary to earlier reports,[20] the rates are *extremely* fast, remain in the fast exchange regime of the NMR time scale even at very low temperatures (−90 °C), and are even faster for low-spin Fe(II) porphyrinates.[14] These results preclude the use of simple model hemes to investigate the effect of axial ligand plane orientation on reduction potentials over the entire liquid range of all common solvents. Thus, specially designed complexes having either covalently attached axial ligands or rigid "pockets" to hold noncovalently attached ligands in fixed orientations will be required to achieve this goal. The preparation of several such iron porphyrinates is in progress in our laboratories.

General Results and Conclusions Concerning the Measurement of Rate Constants from NOESY/EXSY Cross-Peak Intensities. *"Unsymmetrical" EXSY Spectra.* The simple treatment presented herein does not account for differences in cross-peak intensities on the two sides of the diagonal that result from the increasing delays due to the incremented t_1 time domain, although it could in principle be modified to do so. The reason we have not included this effect is that it is expected to be small compared to the experimental error, because it was found that the experimental data showed random differences in cross-peak intensities on the two sides of the diagonal.

Mixing Time. The "flexibility" of k is 10−70%, usually about 30%. The maximum T_1 correction (eq 13) is less than 14%. The quantity $\tau_m k$ is most sensitive in the range 0.1−3.5, usually about 1.5; $\tau_m(k + T_1^{-1})$ is in the range 0.7−4.5, usually about 2. Roughly speaking, both quantities are of the order of 1.0. These results may be compared to those of Perrin,[23] who concluded that $\tau_m = \alpha/(\beta k + T_1^{-1})$, with optimal α and $\beta \sim 1$ for normal noise. However, no comparison of intensities with noise were made in this work. In comparison, Dimitrov and Vassilev[24] investigated a four-site exchange system by 1D and 2D EXSY spectroscopy and concluded that the optimum mixing time was given by the relationship $\tau_m k \approx 0.6$, which is within the range found in this study (Figure 3), although on the low side. It should be remembered that there are also experimental constraints on τ_m itself, based upon the relaxation times, T_1, which become important for paramagnetic complexes, such as the low-spin iron(III) porphyrinates of this study and for investigation of complexes of quadrupolar nuclei such as ^{51}V. Crans and co-workers found that optimum mixing times in this case ranged from $T_1/2 < \tau_m < 3T_1/2$ in their studies of a four-site exchange system having unequal abundances and multiple rate constants.[7] Hence, it is possible that reaction rates and nuclear T_1s may be incompatible to allow measurement of rate constants in some fast-relaxing systems.

Accuracy. First of all, the accuracy in calculation of k is determined by the accuracy of the measurements but not the value of the mixing time. (We have observed "bad" points with "good" mixing times.) This is a natural consequence of the fact that the greater the accuracy, the wider the region of "acceptable" τ_m (see eq 21 and Figure 3). The standard deviations in $\Delta H^{\ddagger}$ and $\Delta S^{\ddagger}$ are the final measure of accuracy.

The initial guess (estimation 12) is very close to the final fitting (within a few percent). It is especially close to the fitting to intensities (method 2), because it is also based on intensities. The reason for this is that the real dispersion of T_1^{-1} is relatively small and correction 13 is only of the second order. Note that estimation 12 is very stable: even for noisy data it gives values of k close to those based on reliable data points, while detailed fittings converge to the noise. Thus, estimation 12 provides a rapid, simple means of estimating the rate constant with relatively high accuracy.

As was mentioned above, the first method of integration underestimates the rate constants and, consequently, overestimates $\Delta H^{\ddagger}$ and $\Delta S^{\ddagger}$. The second method gives the opposite situation. This is in accordance with the results (compare lines 3 and 4 of Table 3).

Acknowledgment. The support of this work by the National Institutes of Health, Grant DK 31038 (F.A.W.), the Materials Characterization Program at the University of Arizona, and the National Science Foundation, Grant CHE-9214383 (for purchase of the Varian Unity-300) is gratefully acknowledged. The authors wish to thank the reviewers for helpful comments.

References and Notes

(1) (a) University of Arizona. (b) On leave from the Institute of Chemical Kinetics and Combustion, Russian Academy of Sciences, Novosibirsk, Russia. (c) On leave from the Boreskov Institute of Catalysis, Russian Academy of Sciences, Novosibirsk, Russia.

(2) San Francisco State University.

(3) Walker, F. A.; Simonis, U. *J. Am. Chem. Soc.* **1991**, *113*, 8652.

(4) Munro, O. Q.; Marques, H. M.; Debrunner, P. G.; Mohanrao, K.; Scheidt, W. R. *J. Am. Chem. Soc.* **1995**, *117*, 935.

(5) Nakamura, M.; Tajima, K.; Tada, K.; Ishizu, K.; Nakamura, N. *Inorg. Chim. Acta* **1994**, *224*, 113.

(6) Ernst, R. R.; Bodenhausen, G.; Wokaun, A. *Principles of Nuclear Magnetic Resonance in One and Two Dimensions*; Clarendon Press: Oxford, U.K., 1992; Chapters 6 and 9.

(7) Crans, D. C.; Rithner, C. D.; Thiesen, L. A. *J. Am. Chem. Soc.* **1990**, *112*, 2901.

(8) Crans, D. C.; Shin, P. K.; Armstrong, K. B. In *Application of NMR Spectroscopy to Studies of Aqueous Coordination Chemistry of Vanadium-(V) Complexes*; Thorp, H. H., Pecoraro, V. L., Eds.; Advances in Chemistry Series 246; American Chemical Society: Washington, D.C., 1995; pp 303−328.

(9) Green, M. L. H.; Sella, A.; Wong, L.-L. *Organometallics* **1992**, *11*, 2650.

(10) Green, M. L. H.; Wong, L.-L.; Selia, A. *Organometallics* **1992**, *11*, 2660.

(11) Alessio, E.; Hansen, L.; Iwamoto, M.; Marzilli, L. G. *J. Am. Chem. Soc.* **1996**, *118*, 7593.

(12) Nakamura, M.; Groves, J. T. *Tetrahedron* **1988**, *44*, 3225.

(13) Momot, K. I.; Walker, F. A. *J. Phys. Chem.* following paper in this issue.

(14) Polam, J. R.; Shokhireva, T. Kh.; Raffii, K.; Simonis, U.; Walker, F. A. *Inorg. Chim. Acta* submitted for publication.

(15) Nesset, M. J. M. Ph.D. Thesis, University of Arizona, 1994.

(16) Nesset, M. J. M.; Shokhirev, N. V.; Jacobson, S. E.; Walker, F. A. Manuscript in preparation.

(17) Watson, C. T. Ph.D. Thesis, University of Arizona, 1996.

(18) Raffii, K. M.S. Thesis, San Francisco State University, 1993.

(19) Miller, J. C.; Miller, J. N. *Statistics for Analytical Chemistry*, 3rd ed.; Ellis Horwood PTR Prentice-Hall: New York, 1993.

(20) (a) Huet, J.; Gaudemer, A. *Org. Magn. Reson.* **1981**, *15*, 347. (b) Cassidei, I.; Bang, H.; Edwards, J. O.; Lawler, R. G. *J. Phys. Chem.* **1991**, *95*, 7186.

(21) Safo, M. K.; Walker, F. A.; Raitsimring, A. M.; Walters, W. P.; Dolata, D. P.; Debrunner, P. G.; Scheidt, W. R. *J. Am. Chem. Soc.* **1994**, *116*, 7760.

(22) Scheidt, W. R.; Lee, Y. J. *Struct. Bonding* **1987**, *64*, 1−70.

(23) Perrin, C. L. *J. Magn. Reson.* **1989**, *82*, 619.

(24) Dimitrov, V. S.; Vassilev, N. G. *Magn. Reson. Chem.* **1995**, *33*, 739.